Lignocellulosic waste biosorbents infused with deep eutectic solvents for biogas desulfurization

Patrycja Makoś-Chełstowska [a,*], Dominika Sikorska [a], Patrycja Janicka [a], Edyta Słupek [a], Aleksandra Mielewczyk-Gryń [b], Jacek Gębicki [a]

[a] Department of Process Engineering and Chemical Technology, Faculty of Chemistry, Gdańsk University of Technology, G. Narutowicza St. 11/12, 80–233 Gdańsk, Poland
[b] Institute of Nanotechnology and Materials Engineering, Faculty of Applied Physics and Mathematics, and Advanced Materials Centre, Gdańsk University of Technology, G. Narutowicza St. 11/12, 80–233 Gdańsk, Poland

ABSTRACT

This paper introduces an innovative method for treating biogas streams, employing lignocellulosic biosorbents infused with environmentally friendly solvents known as deep eutectic solvents (DES). The primary focus of this study was the elimination of volatile organosulfur compounds (VSCs) from model biogas. Biosorbents, including energetic poplar wood, antipka tree, corncobs, and beech wood, were used, each with varying levels of lignin and hemicellulose content. The selection of the DES with the greatest potential for VSC removal was carried out using COnductor-like Screening MOdel for Realistic Solvents (COSMO-RS) modeling. The chosen DES consisted of quaternary ammonium salts and glycols, specifically, tetrapropylammonium bromide and 1,2-hexanediol (1:3). The physicochemical properties of the new DES, such as the viscosity, density, and melting point, were evaluated. The biosorbents were treated with the selected DES after shredding, purifying, and sieving. Comprehensive analysis techniques, including thermogravimetric analysis, scanning electron microscopy, and X-ray diffraction, were employed on the modified biosorbents both before and after modification. The subsequent step involved the adsorption of VSCs from biogas. The results of this study demonstrated the superior performance of a novel sorbent based on corn cob modified by DES compared to commercially available alternatives. The sorption capacity ranged from 103.8 to 112.1 mg/g for various VSCs. The adsorption process using the new biosorbent can be described by the pseudo second order kinetic model, as well as the Yoon-Nelson and Adams-Bohart models. The high efficacy of the VSCs removal was attributed to the concurrent operation of the absorption and adsorption processes. The resulting sorbent was also characterized by its ability to regenerate repeatedly without significant loss of sorption capacity of the new sorbents.

1. Introduction

Biogas serves as an environmentally friendly alternative fuel suitable for heat and electricity generation, as well as for use in transportation. It primarily comprises methane (30-60% v/v) and carbon dioxide (15-50% v/v), alongside additional inorganic impurities like nitrogen, oxygen, water vapor, ammonia, hydrogen sulfide, and a diverse range of volatile organic compounds (VOCs) [1]. The types of organic pollutants encompass aliphatic and aromatic hydrocarbons, siloxanes, volatile organosulfur, and organohalogen compounds, as well as oxygenated organic compounds. It's important to note that the specific composition of biogas heavily relies on the raw materials used for its production.

Among VOCs, volatile organosulfur compounds (VSCs) are particularly troublesome and dangerous. Although VSCs concentrations are considerably lower compared to the major biogas components, they can be problematic in various biogas applications, leading to adverse environmental effects such as stratospheric ozone depletion, contributing to the greenhouse effect, and diminishing local air quality [2]. Additionally, VSCs are substances with highly corrosive properties. When biogas is burned, VSCs can transform into sulfur oxides (SOx). In subsequent stages, SOx can react with water or oxygen, forming highly corrosive sulfuric acid. Consequently, this results in reduced lifespan of equipment within installations, including components of the combustion chamber [3–5].

Given the factors mentioned earlier, biogas purification becomes an essential procedure to safeguard both engines and the environment [6]. Numerous technologies exist specifically for the elimination of VSCs from the gas stream, such as physical absorption, condensation, bio-filtration, and adsorption [3,7–9]. However, a significant drawback for many of these methods is the necessity for toxic solvents, high operational and capital expenses, as well as extended operational durations. Finding alternatives or innovating new techniques in this regard is indeed one of the pivotal challenges faced by the energy industry today.

Processes aiming for high volatile organic compounds (VOCs) removal efficiency are notably characterized by the utilization of conventional adsorbents such as silica gel, activated carbon, and zeolites [10–14]. This efficacy is attributed to their porosity and specific surface area [15]. However, it is imperative to acknowledge that these adsorbents are not without limitations. Challenges in regeneration, limited affinity for polar VOCs among certain conventional adsorbents, finite operational lifespan, low sensitivity to elevated temperatures, and hydrophilic tendencies collectively underscore their constraints. As a response to these limitations, there has been a burgeoning interest in the deployment of a new generation of advanced sorbents, including Metal-Organic Frameworks (MOFs), graphene, carbon nanotubes, and polymeric adsorbents. These materials demonstrate the potential to overcome the drawbacks associated with conventional adsorbents, thereby gaining increased popularity [16–18]. However, the preparation of these advanced sorbents is often intricate, and costly, and necessitates the use of substantial quantities of toxic chemicals [19,20]. In recent years, there has been a notable surge in the popularity of biosorbents derived from waste materials for VOCs adsorption. This emerging trend aligns with the pursuit of sustainable and eco-friendly solutions. The utilization of biosorbents offers a promising avenue for VOC removal, capitalizing on the inherent advantages of waste-derived materials while contributing to environmental conservation. Biosorbents, derived from natural materials such as agricultural waste (i.e. sugarcane bagasse, bark, corn husk, cobe, rice husk, and straw), peels from fruits and vegetables such as bananas, avocados, lemons, oranges, pomegranates, cucumbers, zucchinis, dragon fruits, and seeds from peaches, avocados, or cherries. shells from coconuts or nuts, algae, and animal waste (fish scales, crab shells, and chicken feathers) exhibit excellent adsorption properties due to their porous structures and functional groups. These materials not only provide an environmentally friendly alternative to traditional adsorbents but also contribute to the valorization of biomass residues [21–24]. However, pure biosorbents do not show high removal efficiency of VOCs from the gas phase. Therefore, it is necessary to perform appropriate modification of their surface, i.e. impregnation, or chemical or physical activation [16].

Among the available modification methods, the simplest and most eco-friendly approach is impregnation using the dip-coating method with non-toxic and biodegradable substances. This category of substances includes a new generation of solvents known as deep eutectic solvents (DES). These solvents are obtained by combining two or more chemicals, where one component serves as a hydrogen bond donor (HBD), and the other as a hydrogen bond acceptor (HBA). These components are connected through specific non-covalent interactions, leading to a significant reduction in the melting temperature of DES compared to pure substances. By carefully selecting appropriate HBAs and HBDs, the physico-chemical properties of DES can be easily controlled [25,26]. Due to their unique characteristics, DES has predominantly been utilized for impregnating adsorbents such as silica gel, MOF, and activated carbon, among others, primarily for the adsorption of gases like CO_2, NH_3, or H_2S [27–29]. Only a limited number of studies have demonstrated the effectiveness of modified adsorbents for capturing VOCs [30]. To the best of our knowledge, lignocellulosic DES biosorbents have not yet been investigated for biosorbent coating and application in VOC adsorption from the gas phase.

In this paper, a novel approach is proposed, utilizing the same feedstocks employed in biogas production for its desulfurization. This is the first time deep eutectic solvents have been used as impregnates for biosorbents. This also represents the first time a DES-modified biosorbent has been implemented to desulfurize biogas streams. Four distinct types of lignocellulosic biomass were tested: energetic poplar wood, antipka tree, corncobs, and beech wood. These biosorbents were impregnated with a new DES, aiming to enable the capture of volatile organosulfur compounds from the biogas stream. To identify the most suitable DES, which exhibits a high affinity for VSCs while having no affinity for CH_4, computational modeling using COSMO-RS was conducted. For this purpose, 42 HBA:HBD complexes were tested. The selected DES was then applied to coat the biosorbents. A comprehensive characterization of both the raw and modified biosorbents was performed using SEM, XRD, and FT-IR techniques. Subsequently, these biosorbents were utilized for the removal of volatile organosulfur compounds from a model biogas stream. Regeneration capabilities were assessed, and the potential sorption mechanism of VSCs was elucidated.

2. Materials and methods

2.1. Reagents

The following substances were used to prepare biosorbents impregnated with DES: tetrapropylammonium bromide (purity 98%) and 1,2-Hexanediol (purity 98%) purchased from Merck (Germany), and ethanol with a purity greater than 97% obtained from POCH (Poland). High-purity gases were used for chromatographic studies. Helium (purity N 5.5) was purchased from Linde Gas (Poland). The air was generated by a DK50 compressor with a membrane dryer (Ekkom, Poland), and hydrogen (purity N 5.5) was generated by Precision Hydrogen 1200 Generator (PEAK Scientific, Scotland, UK). Model biogas was purchased from Linde Gas (Poland).

2.2. Methods

2.2.1. DES screening

The ADF COSMO-RS program (SCM, Netherlands) was utilized to assess 42 innovative impregnation layers based on DES. Geometry optimization was carried out for eutectic mixtures comprising a variety of chemical compounds, such as choline chloride (ChCl), tetramethylammonium chloride (TMACl), tetramethylammonium bromide (TMABr), tetraethylammonium chloride (TEACl), tetraethylammonium bromide (TEABr), tetrapropylammonium chloride (TPACl), tetrapropylammonium bromide (TPABr), 1,2-ethanediol (ED), 1,2-propanediol (PrD), 1,4-butanodiol (BD), 1,5-pentanediol (PD), 1,6-hexanediol (HD), and glycerol (Gly). This optimization was executed using the COSMO model with continuum solvation at the BVP86/TZVP level of theory. In the initial stage, the geometry optimization of all DES in the gas phase was performed to identify the most stable conformers. Subsequently, vibrational analysis was conducted to ascertain the DES conformer that truly represented the energy minimum. For the conformer with the highest energy stability, a comprehensive geometry optimization of the DES was carried out.

2.2.2. DES synthesis and characterization

DESs were made by mixing two substances called hydrogen bond acceptor and hydrogen bond donor in a ratio of 1:3 molar. Before the synthesis of DES, all chemical components were dried to remove any moisture. The blend of HBA and HBD was then subjected to magnetic stirring at 80 °C and 1000 rpm until a uniform liquid was achieved. Subsequently, the DES was cooled down to room temperature (RT). The measurements of dynamic viscosity and density for the DES were carried out in a temperature range of 25–60 °C using a BROOKFIELD LVDV-II + viscometer (Labo-Plus, Poland) and DMA 4500 M density meter (Anton Paar, Poland), respectively. The melting point of DES was determined using a visual method, as described in previous studies [31,32]. The DES was cooled to −45 °C in a cryostat and then increased by 1 °C/min until

it transitioned completely from a solid to a liquid state. This was identified as the melting point of DES.

2.2.3. Biosorbents preparation and modification by DES

Various types of lignocellulosic biomass including Energetic poplar wood (EPW) *Populus L.;* Antipka tree (AT) *Cerasus mahaleb;* Corn cobs *(CC) Zea mays;* Beech wood (BW) *Fagus L.;* were used in this studies. Preparation and characterization of the raw biosorbents were performed based on previous work [33]. Lignocellulosic materials were processed by milling and mincing using a Meec Tools garden shredder 425 and RETCH Ultra Centrifugal Mill ZM 200, and subsequently sieved through a 0.75 mm screen. The ground biosorbents were then dried at 105 °C for 4 hours and stored at RT in sealed containers. The analysis of various parameters for each lignocellulosic biosorbent involved determining the ash, extractives, and lignin content of the raw materials, following the analytical procedures outlined by the National Renewable Energy Laboratory (NREL). The cellulose and hemicellulose content were determined using HPLC with a Rezex Pb^{2+} column (dimensions: 300 mm × 7.8 mm, 8 µm) and refractometric detection (Knauer). Elution was carried out with water at a flow rate of 0.6 mL/min [34]. The detailed composition of the biosorbents is provided in Table S1. Biosorbents impregnated with DES were prepared using the dip-coating method based on previous studies [30,35–38]. Raw biosorbents were washed with water or pure ethanol with the assistance of ultrasonic treatment for 2 hours and then dried in a vacuum dryer at 80 °C for 4 hours. Subsequently, the biosorbents were immersed in a 10 wt.% solution of DES in ethanol and shaken for 2 hours at room temperature. The ethanol was then decanted, and the remaining solvent was evaporated from the biosorbents using a vacuum dryer.

2.2.4. Characterization of biosorbents

Various methods were employed to characterize the surface and functional properties of the newly developed lignocellulosic biosorbents that had been modified with DES.

Fourier transform infrared spectroscopy with attenuated total reflection was carried out using a Tensor 27 spectrometer (Bruker, USA) and OPUS software (Bruker, USA). This allowed for the examination of the structural composition, identification of chemical bonds, and determination of the main functional groups present on the biosorbents' surface. The analysis was conducted within a spectral range of 4000-600 cm^{-1}, with a resolution of 4.5 cm^{-1}, 256 sample scans, 256 background scans, and a slit width of 0.5 cm.

X-ray powder diffraction measurements were performed at room temperature using CuKα radiation and a Philips X'Pert Pro diffractometer. The study covered both pristine and modified biosorbents in the range of 10–90° with 0.01° steps and the scanning speed was set at 1°/min.

For investigating the surface morphologies, a scanning electron microscope (SEM) FEI Quanta 250 FEG (Thermo Fisher Scientific, Waltham, MA, USA) was utilized, studying both the pristine and modified lignocellulosic biosorbents.

Additionally, thermal analysis of the samples was conducted using a simultaneous thermal gravimetric (TG) and differential thermal gravimetric (TG/DTG) analyzer, specifically the Netzsch TG 209 F3 Tarsus in nitrogen (Selb, Germany).

2.2.5. Adsorption and regeneration processes

To verify the effectiveness of the newly developed biosorbents in adsorbing volatile organosulfur compounds, the laboratory setup shown in Figure 1 was employed. A model biogas mixture consisting of methane (CH_4) at 60.2% v/v, carbon dioxide (CO_2) at 30.0% v/v, nitrogen (N_2) at 9.8% v/v, as well as specific trace amounts of carbon disulfide (CS_2) at 11.6 ppm, dimethyl disulfide (DMDS) at 11.8 ppm, 1-propanethiol (PM) at 11.3 ppm, and 2-propanethiol (IPM) at 11.5 ppm was introduced into the adsorption column. The flow rate of biogas was set at 25 mL/min, and the column contained 0.8 grams of the new biosorbent. These tests were conducted under room temperature conditions and at a pressure of 1 atm. Two sampling points were placed in the installation, one before and one after the adsorption column, to monitor the effectiveness of VSCs removal from the gas mixture. The samples collected were analyzed using gas chromatography coupled with a flame photometric detector (GC-FPD). The analysis employed a GC Clarus 580 instrument (PerkinElmer, USA) with a capillary column (ELITE-1MS, dimensions: 60 m × 0.32 mm × 1.0 µm) manufactured by (PerkinElmer, USA).). The temperature program for chromatographic analysis was as follows: first stage - initial oven temperature 40 °C (for 1 min); second stage - increase at a rate of 30 °C /min to a temperature of 100 °C; third stage - increase at a rate of 45 °C /min to a temperature of 250 °C, which was maintained for 3 minutes. Moreover, the injection port temperature was maintained at 250 °C, a split injection mode with a
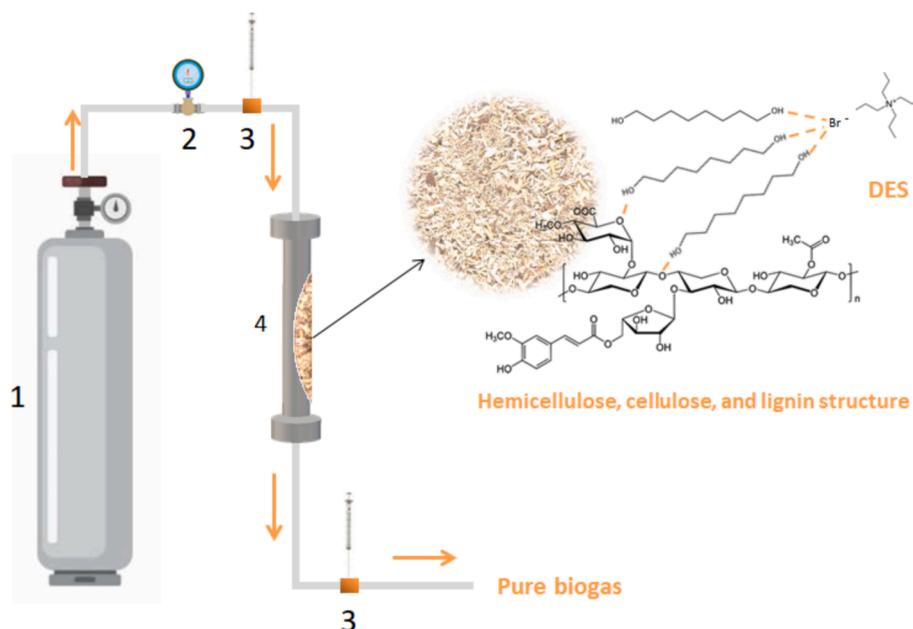
Fig. 1. Laboratory adsorption set-up a) bottle with model biogas; b) flow meter; c) sample collection point; d) adsorption column.

ratio of 5:1, the detector temperature was set to 300°C, and helium was utilized as the carrier gas with a flow rate of 2 mL/min. The volume of the injected sample was 2.5 mL. Additionally, an analysis of the composition of key biogas components, specifically CH_4 and CO_2, was conducted using gas chromatography coupled with a thermal-conductivity detector (GC-TCD). A GC Clarus 680 instrument (PerkinElmer, USA) equipped with a packed column (Porapack Q, dimensions: 80/100, 2 mm ID) supplied by (PerkinElmer, USA) was employed for this purpose. The conditions for this analysis included an oven temperature set at 40°C, injection port temperature at 60°C, detector temperature at 80°C, helium utilized as the carrier gas with a flow rate of 5 mL/min, and a sample injection volume of 0.25 mL.

The concentrations of VSCs at the inlet (C_{IN}, mg/m³) and outlet (C_{OUT}, mg/m³) were monitored every 30 minutes to track breakthrough curves, which depict the changes in C_{OUT}/C_{IN} over time until adsorption equilibrium was achieved. In this investigation, the breakthrough time was defined as the moment when the concentration of VSCs at the outlet reaches 5% of the concentration at the inlet [39,40]. The dynamic adsorption capacity (q_e, mg/g) of VSCs was calculated using Eq. (1).

$$q_e = \frac{F}{m} \bullet \int\limits_0^t (C_{IN} - C_{OUT}) \bullet dt \tag{1}$$

where: F – model biogas flow rate (m³/min).

m – mass of biosorbents (g).

t - breakthrough time (min).

To assess the efficacy of pristine biosorbents and DES-biosorbents in adsorbing VSCs, the pseudo-first order (PFO) (Eq. (2), pseudo-second order (PSO) (Eq. (3), Elovich (Eq. (4), and intraparticle diffusion (IPD) (Eq. (5) adsorption kinetic models [41,42] were adopted.

$$q_t = q_e \bullet [1 - e^{(-K_1 t)}] \tag{2}$$

$$q_t = \frac{K_2 \bullet q^2 \bullet t}{1 + K_2 \bullet q \bullet t} \tag{3}$$

where: K_1 and K_2 – reaction constants of the pseudo-firs and pseudo-second order equations, respectively (1/min).

q_t – adsorption capacity of VSCs at any adsorption time (t, min) (mg/g).

$$q_t = \frac{1}{\beta} \bullet \ln(\alpha\beta) + \frac{1}{\beta} \bullet \ln t \tag{4}$$

where: α - initial adsorption rate constant (mg/(g·min)).

β - desorption constant related to the surface coverage and adsorption activation energy (g/mg).

$$q_t = K_{IPD} \bullet t^{\frac{1}{2}} + C \tag{5}$$

where: K_{IPD} - intra-particle diffusion rate constant for adsorption (g/mmol·min$^{1/2}$).

C - intercept that represents the boundary layer thickness (mg/g).

The credibility of the kinetic models was evaluated using the correlation coefficient (R^2) values and normalized standard deviation Δq (%), which was determined using Eq. (6).

$$\Delta q = 100 \bullet \sqrt{\frac{\sum \left[\frac{q_e - q_{mod}}{q_e}\right]^2}{N - 1}} \tag{6}$$

Where: q_{mod} - adsorption capacity of kinetic models (mg/g).

N - the number of adsorption kinetics data points.

To better understand the adsorption processes of the VSCs in the fixed bed, three dynamic adsorption models including Yoon-Nelson (Eq.

(7), Thomas (Eq. (8), and Adams-Bohart (Eq. (9) were adopted.

$$\frac{C_t}{C_0 - C_t} = \exp(K_{YN}t - \tau K_{YN}) \tag{7}$$

where: K_{YN} - rate constant (1/min);

τ - time required for 50% adsorbate breakthrough (min);

C_0 – VSCs concentration in an initial gas stream (mg/mL);

C_t – VSCs concentration in outlet gas (mg/mL).

$$\frac{C_t}{C_0} = \frac{1}{1 + \exp\left[\left(\frac{K_{Th} \bullet q_e \bullet m}{F}\right) - K_{Th} \bullet C_0 \bullet t\right]} \tag{8}$$

where: K_{Th} - Thomas model constant (mL/(min·mg));

q_e (mg/g) is the predicted adsorption capacity.

$$\frac{C_t}{C_0} = \exp(K_{AB}C_0 t - K_{AB}N_0\frac{Z}{U_0}) \tag{9}$$

where: K_{AB} – rate constant of Adams-Bohart model (L/(min·mg));

z - the bed depth (cm);

N_0 - maximum VSCs adsorption capacity per unit volume of adsorbent column (mg/L);

U_0 - linear velocity of gas stream (cm/min).

Pristine biosorbents and DES-biosorbents were regenerated after adsorption process. The desorption process was performed by heating at 100°C for 2 h. The efficiency of pristine biosorbents and DES-biosorbents regeneration (ER, %) was calculated using Eq. (10).

$$ER = \frac{q_{(n)}}{q} \bullet 100\% \tag{10}$$

where: $q_{(n)}$ – dynamic adsorption capacity of VSCs at n-cycle.

3. Results

3.1. DES preselection

In this study, an exhaustive screening process was conducted on a set of 42 DES. The primary objective was to identify DES demonstrating superior efficacy in dissolving four specific VSCs, thereby enhancing sorption capacity of the obtained sorbents by combining adsorption on the sorbent surface and absorption in the volume of DESs. By combining the sorbent and DES sorption abilities, it is possible to obtain an exceptionally effective material for gas separation. VSCs compounds were selected based on the composition of the actual biogas streams. The composition of biogas and content of individual VSCs vary depending on the biogas feedstock used. However, CS_2, DMDS, PM, and IPM can be identified in almost all types of biogas streams [43].

The computations were executed utilizing binary eutectic complexes with a molar ratio of 1:3. Seven quaternary ammonium salts (QASs), namely ChCl, TMACl, TMABr, TEACl, TEABr, TPACl, and TPABr, were evaluated as HBAs in conjunction with various glycols (HBDs) such as ED, PrD, BD, PD, HD, and Gly. The solubility outcomes for individual VSCs including CS_2, DMDS, PM, and IPM are illustrated in Figure 2. The findings indicate that the solubility of VSCs in DES increases with the extension of the alkyl chain in the QASs' structure. This observation aligns with prior research, highlighting the pivotal role of weaker van der Waals interactions, specifically C-H···S, in influencing the solubility of VSCs, such as sulfides, in DES. Notably, hydrogen bonds between the sulfur atom and the hydroxyl group do not form, as evidenced in previous studies [44]. Consequently, ChCl exhibited the lowest solubility among the tested QASs. Similar trends were observed for various HBDs, where glycols with longer alkyl chains displayed greater affinity for VSCs, although the impact was less pronounced compared to HBAs. Furthermore, the influence of the anion in HBAs on the dissolution efficiency of sulfur compounds was investigated. However, the

Fig. 2. Matrix of solubility screening of volatile organosulfur compounds, CH_4, and CO_2 in DES based on COSMO-RS model.

calculations revealed only marginal enhancement in solubility when employing Br^- ions. The hydroxyl groups from glycols have the capability to engage in hydrogen bonding with the mercaptan group, leading to the formation of HO···HS interactions. Consequently, the solubility of mercaptans is notably elevated in comparison to the sulfides examined. Among the various DESs assessed, TPABr:HD (1:3) exhibited the highest efficacy in solubilizing all VSCs.

Another parameter considered was the low solubility of the main components of biogas, namely, methane and carbon dioxide. Methane is the target product obtained after biogas purification. In contrast, the high solubility of carbon dioxide would saturate the active groups that determine the removal of VSCs. In addition, many solutions are

currently available for the efficient removal of CO_2 from biogas. The results show that all tested DESs exhibit very low solubility of the CH_4 which are 0.33–0.44 g/L, and relatively low solubility of the CO_2 in the range of 3.5–4.6 g/L All DES showed about 10-fold higher sorption capacity for CO_2 than for methane. This is due to the presence of two atoms that can form hydrogen bonds with the hydroxyl groups of the HBDs. However, their solubility is much lower than that of VSCs, which range from 209.9 to above 2000 g/L.

Another crucial parameter for ensuring the utility of DES as biosorbent-impregnating substances is their vapor pressure. It is generally acknowledged that DES exhibit low vapor pressure; however, there are few studies in which this property has been measured or calculated

[45,46]. The vapor pressure of DES should be as low as possible to prevent vaporization during gas purification or regeneration. The evaporation of DES from the surface of the sorbents can completely alter the functional properties of the biosorbents and introduce DES components into purified biogas. Given that the regeneration processes are conducted at elevated temperatures, calculations were performed for temperatures ranging from 20 to 70°C (Figure S1). The results indicated that the DES composed of TMABr or TMACl exhibited the highest vapor pressures. The vapor pressure of the DES decreased with an increase in the alkyl chain length. A similar trend was observed for hydrogen bond donors (HBDs), which was attributed to the partial vapor pressures of the individual components. Therefore, the lowest vapor pressures of 0.044 and 0.046 Pa were obtained for TPABr:HD (1:3) and TPACl:HD (1:3), respectively. Furthermore, the vapor pressures are temperature dependent and always increase with increasing temperature. For the same DES, the vapor pressures at 70°C are 46.1 and 46.4 Pa, respectively. Furthermore TMACl:HD (1:3) and TMABr:HD (1:3) showed 468 and 471 % higher vapor pressures at 70 °C compared to TPACl:HD (1:3) and to TPABr:HD (1:3). Therefore, TPABr:HD (1:3) was exclusively selected for subsequent investigations.

To deepen comprehension and validate the previously posited hypotheses concerning the interaction between DES and VSCs, the assessment of σ-profiles was conducted by employing 3D surface charge densities [47]. The σ-profiles results for both DES and VSCs are presented in Figure 3. The σ-profile graph was partitioned into three distinct interaction domains: a non-polar region spanning the range of -0.0084 e/A^2 > σ < 0.0084 e/A^2, a hydrogen bond donor region (σ < -0.0084 e/A^2), and a hydrogen bond acceptor region (σ > 0.0084 e/A^2) [35,48–50].

The ability of the examined components to participate in strong hydrogen bonding is emphasized by both the regions acting as hydrogen bond donors and acceptors. Notably, consistent outcomes were observed across all VSCs. The primary peak was identified in the nonpolar region, with smaller peaks apparent in the hydrogen bond acceptor regions due to the presence of sulfur atoms. In TPABr:HD (1:3), the largest peak is also situated in the nonpolar region, accompanied by peaks in the HBA and HBD regions. This occurrence is attributed to the active -OH and Br- groups in the DES structure, suggesting the potential for both hydrogen

bonding and weaker non-covalent interactions with VSCs. Furthermore, previous investigations have highlighted the significance of compatible -profiles between DES and VSCs, involving identical regions, an increase in the σ-profile for one compound, and a corresponding decrease for the other. These factors are crucial for establishing robust molecular interactions [51]. Collectively, these findings strongly suggest significant potential for the adsorption of VSCs using DES-biosorbents.

3.2. Synthesis and physical properties of DES

According to COSMO-RS modeling, TPABr:HD (1:3) was deemed the most suitable DES for biosorbent coating. To gain an understanding of the physicochemical properties of this novel DES, its density and viscosity were measured from 25 to 60 °C, and its melting point was also determined. Although there is limited literature available on these properties, these measurements were conducted to provide essential information about the fundamental properties of the DESs. The results of the density and viscosity tests are shown in Figure. S2.

Density is a common property used for characterizing DESs, as it significantly affects numerous technological processes. Generally, the densities of DESs are temperature dependent and typically higher than those of water. At 25 °C, the DES density was 1.01148 g/cm^3. As anticipated, Figure S2 shows that the density of the DES decreased as the temperature increased. This trend can be attributed to the increased activity and molecular mobility, which lead to an increase in the molar volume of the solution and a consequent reduction in density [52–56].

Dynamic viscosity is a crucial parameter for solvents in various industrial processes involving fluid flow systems. Most DESs exhibit higher viscosity (>100 cP) than water and traditional solvents, which can pose challenges in pumping, filtering, or stirring. However, when DES is used as an adsorbent impregnant, a relatively high viscosity is desirable. A higher viscosity improves the adhesion of the DES to the sorbent surface, resulting in modified sorbents with improved durability, stability, and lifespan. The results showed that the viscosity of the DES at 25 °C was 105.2 mPas. Additionally, similar to the density, the dynamic viscosity is significantly influenced by temperature. As the temperature increased, the viscosity of the DES decreased significantly. This is because an increase in the DES temperature leads to an increase in the average speed
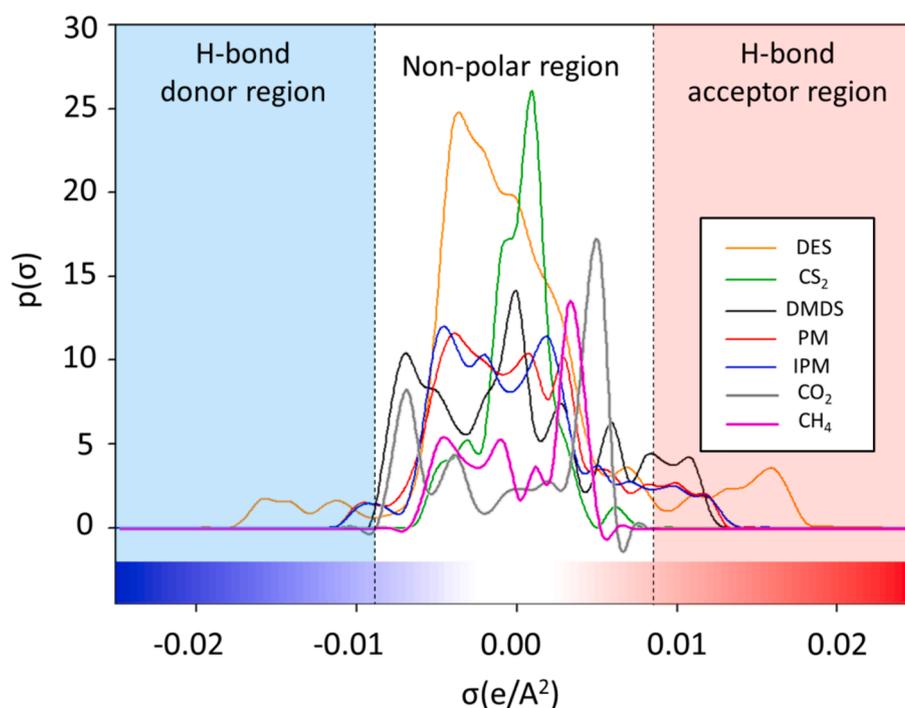
Fig. 3. σ-profiles of TPABr:HD (1:3), CH$_4$, CO$_2$ and VSCs including CS$_2$, DMDS, PM and IPM.

of the molecules in the liquid phase, which reduces the intermolecular forces. This reduction in force can decrease the fluid's resistance to flow (dynamic viscosity) [52–55,57].

The Melting point (MP) of the pure compounds including TPABr and HD, were 270 °C and 2 °C, respectively. In the DES complex, a significant depression of MP compared to that of the pure compounds was observed. The melting point of the new DES was below -40 °C, indicating the formation of a deep eutectic solvent.

3.3. Biosorbents preparation and characterization

The raw biosorbents were then subjected to an impregnation process using the selected DES. Then for all biosorbents before and after the impregnation process, detailed characterization was carried out.

The morphologies of the biosorbents before and after DES impregnation were studied by Electron Microscopy. The SEM results are shown in Figures 4 and S9. No differences were observed between the sorbents purified using water and ethanol. Therefore, only the microscopy results after water purification were included in this study. Figure 4 shows that the pristine corn cob was characterized by a partially porous and smooth structure. After DES impregnation, a thin layer of DES was observed. This proves that the biosorbent was heavily coated with DES. The surface remained porous, and additional active sites containing DES appeared on the surface of the corncobs. Similar results were obtained for the other adsorbents. In contrast, the single open pores present on the surface of the treated sorbents were completely clogged with DES, which may have prevented VSCs from penetrating the pores.

FT-IR analysis was conducted on all biosorbents, both before and after modification with DES. The aim was to ascertain the principal
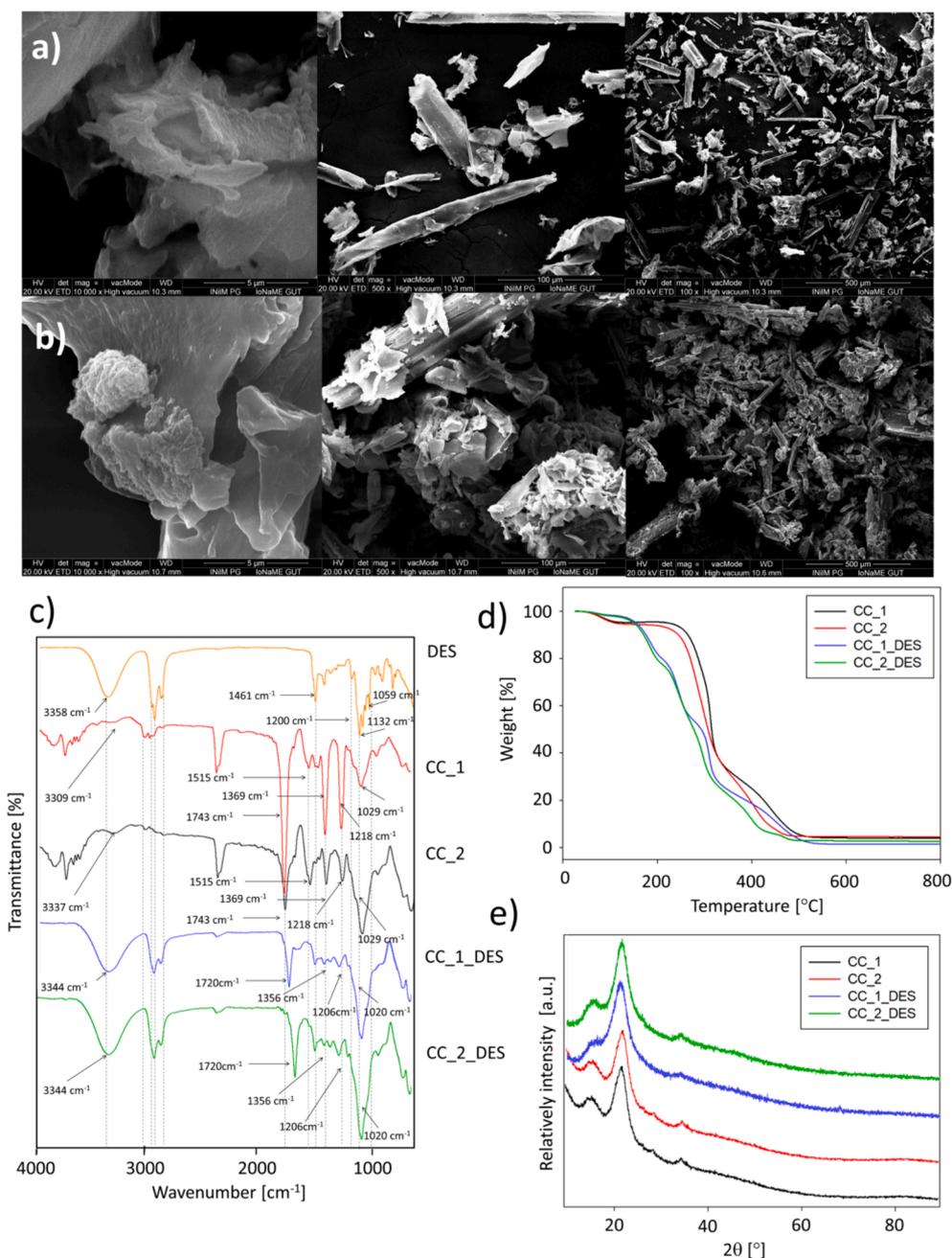
Fig. 4. Characterization of pristine corn cobs biosorbents and DES-corn cobs biosorbents: a) SEM images of corn cobs biosorbents treated by water (CC_1); b) SEM images of corn cobs biosorbents impregnated by DES (CC_1_DES); c) FT-IR spectra; d) TG curves; e) X-Ray Diffraction (XRD) patterns.

functional groups present on the sorbent surfaces and to gain insight into the binding mechanisms between DES and lignocellulosic biosorbents. The outcomes of this analysis are presented in Figures 4 and S9. In the FT-IR spectra of the pure lignocellulosic biosorbents, a broad peak was evident between 3309 to 3341 cm⁻¹. The position of this peak and its intensity exhibit slight variations depending on the specific biosorbent being tested. These discrepancies arise from differences in the constituent components, namely, cellulose, hemicellulose, lignin, and water content. Furthermore, the choice of extraction solvent also contributes to shifts in the position of the ν(O-H) band. When inspecting spectra from biosorbents extracted with water, the band's position is notably shifted to lower wavenumbers. This shift can be attributed to the presence of residual solvent within the sorbent's structure. Additionally, two sets of peaks arise from C-H asymmetric and symmetric stretching and are located in the spectral range of 2878 to 2930 cm⁻¹. Further along the spectra, prominent bands appear at 1743, 1515, 1369, 1218, and 1029 cm⁻¹. These originate from unconjugated C=O groups, predominantly found as acetyl groups within hemicelluloses. Furthermore, the spectra display aromatic skeletal vibrations characteristic of lignin, syringyl ring breathing coupled with CO stretching, C-O vibration within syringyl derivatives of lignin, and C-H vibrations within cellulose. Additionally, signals corresponding to C-O stretches in both lignin and xylan are observed, along with syringyl ring vibrations and C-O stretching of primary alcohols in cellulose and hemicelluloses, respectively [58,59]. In the spectra of all biosorbents modified with DES, additional bands arising from the impregnant's structure become apparent. Within the spectrum of unadulterated DES, a distinctive broad band emerges at 3358 cm⁻¹, originating from the convergence of the O-H stretch from the HBD and the N-H stretch from the HBA. Furthermore, prominently intense peaks can be discerned at 1200, 1132, and 1059 cm⁻¹, corresponding respectively to the C-O-C vibration, the stretching vibration of C-O bonds, and the stretching of C-OH groups. [60,61]. In the spectra of the modified biosorbents, shifts in characteristic bands within the O-H stretch domain are discernible, displaying a displacement towards lower wavenumber values compared to pure DES and conversely towards higher values in comparison to unmodified biosorbents. Additionally, bands originating from the C-O stretch in lignin and xylan, the syringyl ring, and the C-O stretch of primary alcohols within cellulose and hemicelluloses also exhibit shifts toward lower values. These observations suggest that DES interacts with the structure of lignocellulosic biosorbents through hydrogen bonds. Specifically, hydrogen bonding occurs between a hydroxyl group from the DES and oxygen atoms (C-O···HO) within the components of lignin, cellulose, and hemicellulose.

The thermal stability of both clean and modified biosorbents was studied using thermogravimetric analysis (TGA). The TGA diagrams, obtained by heating the samples from 20 to 800 °C at a rate of 10 °C/min, are shown in Figures 4 and S9. Under an air atmosphere, all pristine biosorbents displayed four mass loss stages. In the first stage, occurring between 100-110 °C, a water loss in the range of 3.3 – 4.8 % was observed. Higher mass loss values were observed for pure biosorbents due to their relatively hydrophilic nature. However, the modified biosorbents, which had a hydrophobic layer applied to the surface, showed lower mass loss due to water evaporation. During the following stage, a reduction in mass was noticed at temperatures ranging from 250 to 325 °C, signifying the decomposition of hemicellulose. Subsequently, a more pronounced mass loss occurred at 320-400 °C, attributed to the degradation of cellulose. At temperatures above 400 °C, the degradation of lignin was observed. Notably, the phenolic hydroxyl group, indicative of the presence of lignin, enhances thermal stability and facilitates lignin degradation at elevated temperatures [62,63]. The results indicate that the method of preparation of biosorbents does not have any significant effect on the thermal stability of the new adsorbents. In the TGA curves of DES-modified biosorbents, two additional mass losses can be observed in the ranges from 160 to 225 °C and from 225 to 270 °C, which are attributed to the degradation of DES components, including TPAB and 1,8-HDOL. Since the same DES and its concentration were used to impregnate the sorbents, and the lignocellulosic biosorbents have very similar compositions, their TGA diagrams closely resemble each other. This similarity further suggests that the thermal resistance of all tested biosorbents is highly comparable.

X-ray diffraction was employed to assess the crystallinity and physical structure of the lignocellulosic biosorbents before and after being modified with DES. The outcomes of this analysis are displayed in Figures 4 and S9. The diffractograms of the pristine biosorbents exhibit two distinct peaks. The first peak at 18.7° corresponds to the amorphous constituents such as cellulose, hemicellulose, and lignin. The second peak at 22.5° corresponds to α-cellulose [64]. Interestingly, after the modification of the biosorbents, the diffractograms remained unchanged, with no additional peaks emerging within the studied range. Furthermore, the intensity ratio of the peaks identified in the pure biosorbents did not undergo any alteration. These experimental findings provide evidence that the surface modification with DES does not lead to significant structural transformation of cellulose.

3.4. Adsorption processes

3.4.1. Selection of type of DES-biosorbents

In the subsequent part of the study, both pristine and DES-impregnated biosorbents were employed to adsorb VSCs from a model biogas stream. To identify the most effective biosorbent, a comparative analysis was conducted by introducing 0.8 g of pure biosorbent and DES-impregnated biosorbent into an adsorption column, through which the contaminated model biogas was passed (25 mL/min). The concentrations of various substances at the inlet and outlet of the column were measured using gas chromatography. Based on these measurements, the sorption capacity of all sorbents was calculated. The results, illustrated in Figure 5, indicate that impregnating the surface with DES significantly enhanced the adsorption performance for all types of biosorbents. This improvement is attributed to the concurrent processes of adsorption within the biosorbent and absorption within the DES layer on the biosorbent's surface. The thin layer of DES forms non-covalent bonds with the VSCs. Furthermore, the preparation method of sorbents influences the sorption capacity, with sorbents extracted using water demonstrating higher adsorption capacity compared to those washed with ethanol. This difference is likely due to the leaching of various surface compounds that can bind to the VSCs. Among the various sorbents tested, the DES-corncobs treated with water (CC_1_DES) exhibited the highest sorption capacity. The sorption capacities of the individual VSCs were 108.3, 103.8, 105.9, and 112.1 mg/g for CS_2, IPM, PM, and DMDS, respectively. All modified and unmodified biosorbents showed the highest ability to capture DMDS. This is probably due to the presence of two sulfur atoms, which can form strong non-covalent bonds with the DES and the adsorbent surface, that is, O-H···S and C-H···S. At the same time, the presence of two methyl groups can also result in additive weaker interactions with the active groups on the surface of the biosorbent [44,65].

During the adsorption processes, the contents of the main components of the model biogas stream, namely, methane, carbon dioxide, and nitrogen, were also controlled. The sorption capacities are shown in Figure S6. As expected, none of the modified or unmodified biosorbents adsorbed nitrogen. In contrast, sorption of carbon dioxide and methane was observed when BW_1, BW_2, and AT_1 were used. However, subjecting the surface to impregnation with DES significantly decreased the sorption efficiency of the main components. Therefore, the removal of CO_2 from biogas streams is desirable. However, the higher affinity of CO_2 for the sorbent contributes to a decrease in the sorption efficiency of the VSCs. The main components, including CH_4 and CO_2, are broach active groups to which volatile sulfur compounds can attach. In addition, methane sorption is a negative phenomenon because, according to this assumption, the sorbent should not absorb more than 1% v/v methane [32]. The effect of the biosorbent purification process on the sorption efficiency of the VSCs can also be observed from the results
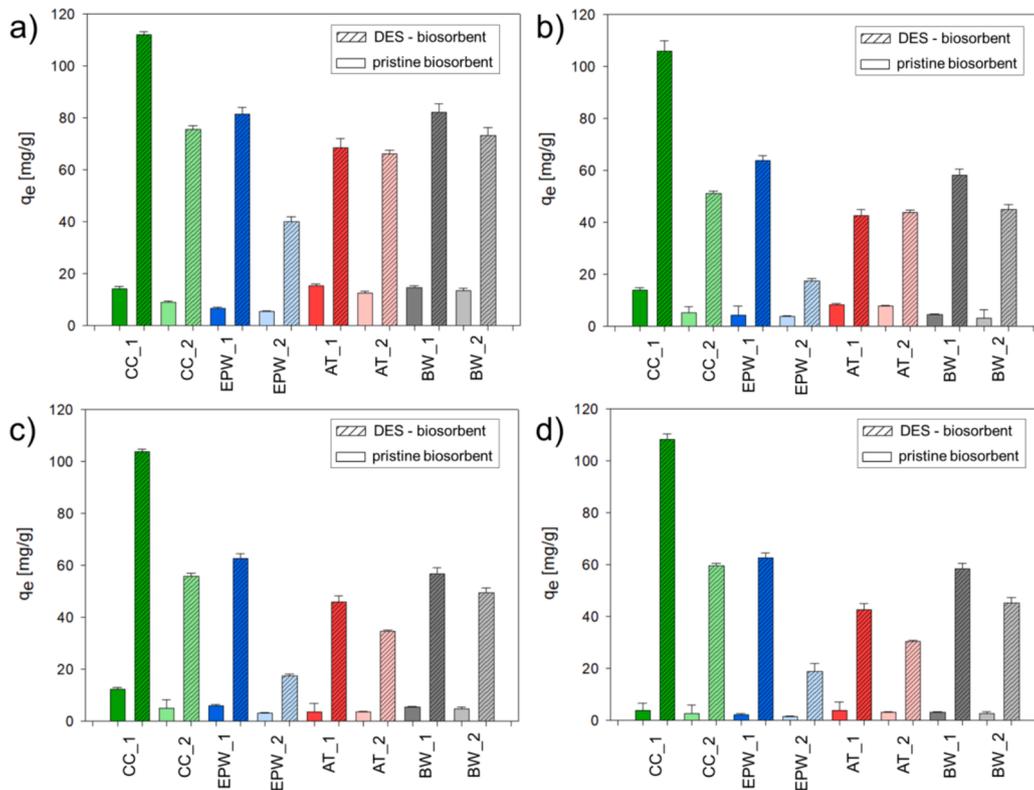
Fig. 5. Adsorption capacities of biosorbents (corn cobs treated by water (CC_1) and ethanol (CC_2); , energetic poplar wood treated by water (EPW_1) and ethanol (EPW_2), antipka tree treated by water (AT_1) and ethanol (AT_2); beech wood treated by water (BW_1) and ethanol (BW_2) towards individual VSCs a) DMDS; b) PM; c) IPM; d) CS_2.
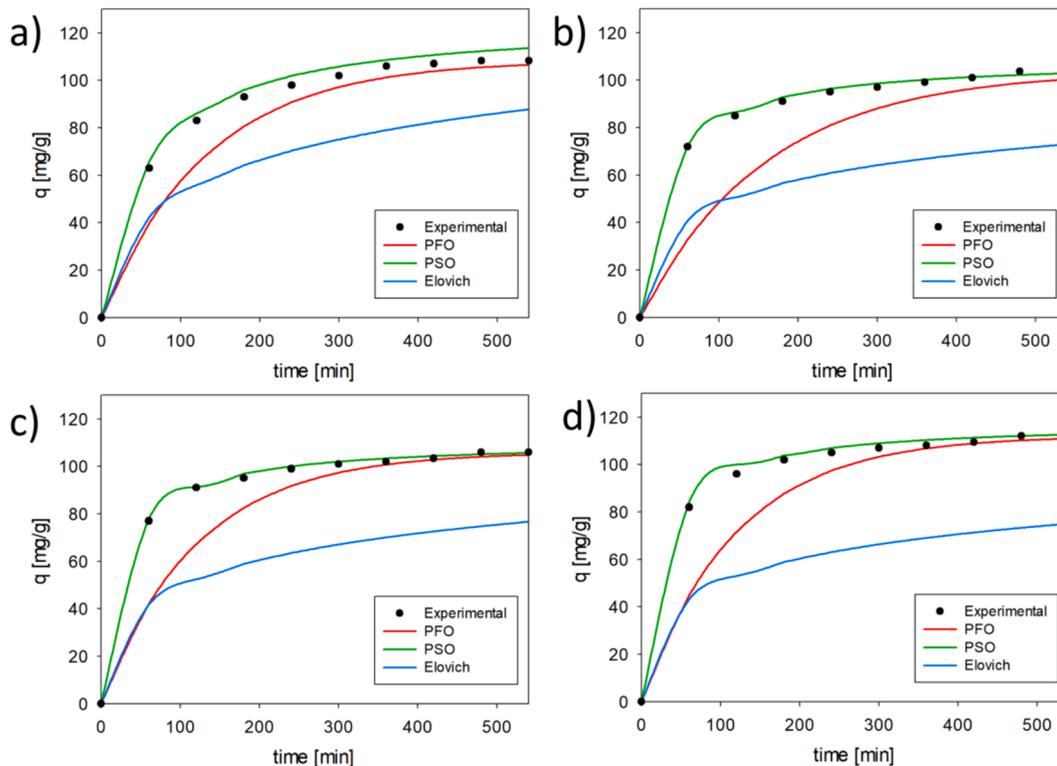
Fig. 6. The kinetic fitted models of a) CS_2, b) IPM, c) PM, and d) DMDS.

obtained. Sorbents treated with water without impregnation, such as CC_1, EPW_1, AT_1, and BW_1 after impregnation, showed a higher sorption capacity. This is due to the more efficient dissolution and removal of contaminants (inorganic substances) that do not contain groups capable of binding to VSCs. In addition, ethanol also partially dissolves the sugars in the biosorbent, which also attaches to VSCs and determines better binding to DES. This is beneficial from an environmental and economic perspective, as water is an easily accessible, cheap, and non-toxic solvent.

As CC_1_DES had the highest sorption capacity, the corn-cob-based biosorbent was used for further analysis.

3.4.2. Adsorption kinetic and modeling

In this part of the study, CC_1_DES was utilized to explore the dynamic adsorption behavior. Figure 6 presents the breakthrough curves and saturation adsorption capacities of the VSCs adsorbed on the new sorbent. The results indicate that all breakthrough curves can be divided into three distinct phases. The first phase involves effective VSCs adsorption. The second phase is characterized by a breakthrough bed (where the adsorbent no longer adsorbs VSCs), and the third phase is reached when the adsorption capacity of the bed in the adsorption column is attained. Only a minimal amount of sulfur compounds was detected in the first phase, suggesting that the biosorbent-modified DES could effectively and rapidly adsorb onto VSCs. The results show that at the beginning of the process, there are active sites on the surface of the adsorbents, which are gradually occupied by VSCs, until the saturation state is approached and there is a significant slowdown in the adsorption of VSCs. Three kinetic models including PFO, PSO, and Elovich, were used to confirm the above assumptions. The PFO model examines the connection between the variation in time and the adsorption capacity on the order of one. The PFO model posits that at the outset, there are no VSCs (adsorbate) present at the surface of the adsorbent; however, with time, the VSCs occupy the surface of the adsorbent. The PSO model is based on the premise that the rate-limiting step is chemical sorption or chemisorption and predicts the behavior across the entire range of adsorption. Under these circumstances, the adsorption rate is dependent on the adsorption capacity and not on the concentration of the adsorbate. The Elovich model is a kinetic model that describes adsorption systems based on their chemical natures. This model occurs when adsorption involves a chemisorption reaction on the adsorbent surface, and the adsorption speed decreases as time passes because of the coverage of the adsorbent surface with the adsorbate [66,67]. The predicted kinetic parameters for CC_1_DES are listed in Table 1. The fitting plots are depicted in Figure 6.

The results obtained from the data suggest that, among the kinetic models, the PSO model provides the best fit for most VSCs. The PSO

model's high R^2 value (above 0.97) and low Δq (below 1.72%) contributed to its status as the best-fitting kinetic model. The PSO model's findings indicate that the adsorption of VSCs onto CC_1_DES occurred primarily through monolayer adsorption via the electron exchange process. While the PFO model also fits the experimental data well, with high R^2 values (above 0.93), the PSO model outperforms CS_2. This suggests that the adsorption of CS_2 on CC_1_DES was mainly controlled by physical adsorption rather than chemisorption. The rate constant is a measure of the speed at which sorption equilibrium can be achieved, serving as a time-scaling factor. In this context, the rate constants K_1 and K_2 derived from the PFO and PSO models were utilized to assess the adsorption rates. As presented in Table 1, the rate constants for PM and DMDS are higher than those for CS_2 and IPM, implying that a shorter time is necessary for the adsorption of PM and DMDS vapors to attain equilibrium. Furthermore, the lower values of K_2 as compared to K_1 confirm that chemisorption was not the rate-determining step. The lowest fit was obtained for the Elovich kinetic model with R^2 values ranging from 0.77 to 0.87, and Δq values ranging from 6.7 to 11.7%. The Elovich model suggests that the adsorption process involves chemical forces acting on a heterogeneous surface. Therefore, the data fit proposes that only non-covalent bonds, such as electrostatic interactions, van der Waals bonds, or hydrogen bonds, are formed between the DES-modified biosorbent and VSCs. As shown in Table 1, all values of β were lower than those of α, indicating that the adsorption rates of all VSCs were higher than their desorption rates.

3.4.3. Mechanism of adsorption mass transfer

Next part of the investigation, an intraparticle diffusion kinetic model (IPD) based on the Weber-Morris equation (Eq. (8)) was used to determine the rate-controlling step of the VSCs adsorption. When the linear plot passes through the origin (C=0), intraparticle diffusion is the rate-controlling step, and film diffusion is negligible. However, if the straight line does not pass through the origin, there is a difference in the rates of mass transfer in the initial and final adsorption steps. This implies that film diffusion is simultaneously involved in intraparticle diffusion [68,69].

The results displayed by the low R^2 values, which range between 0.72 and 0.77, indicate the presence of the multi-linearity with varying slopes, indicating multi-stage adsorption of VSCs on CC_1_DES. The multistage adsorption behavior of organic contaminants on adsorbents has been documented previously [70]. Several factors limit the adsorption kinetics of the adsorbate on the adsorbent, including the diffusion coefficient of the adsorbate in the bulk phase, concentration of the adsorbate, degree of mixing, gas matrix, and the impregnation layer. For each VSCs, three stages with different adsorption rates (i.e., different slopes) were observed. The first stage suggests interactions with the DES. The second stage represents intraparticle diffusion, where the vapor VSCs molecules diffuse into the macropores and wider mesopores of CC_1_DES. The third stage corresponds to the final equilibrium stage, where the vapor molecules penetrate the narrower mesopores and micropores of CC_1_DES. The equilibrium stage occurs rapidly and is not considered to be a rate-limiting step. These findings suggest that both the DES film and intraparticle diffusion processes play significant roles in controlling the rate of adsorption in biosorbents modified with DES. Figure 7 depicts a schematic of the mass transfer mechanism in the adsorption process using CC_1_DES.

3.4.4. Column breakthrough analysis

The design of fixed-bed columns relies on estimating the shape of the breakthrough curve and determining the breakpoint, which are critical aspects for determining the practicality of using adsorbents in real-world applications. To comprehend the behavior of fixed-bed columns and scale them up for industrial applications, it is necessary to have an appropriate model. Several simple mathematical models have been developed to describe and estimate the dynamic behavior of performance in a bed column [71–74]. This study employed three

Table 1
Kinetics model parameters for the VSCs adsorption on CC_1_DES

Kinetic model	Parameter	CS_2	IPM	PM	DMDS
PFO	q_e (mg/g)	106.5	100.4	104.8	110.9
	K_1 (1/min)	0.0076	0.0063	0.0084	0.0085
	R^2	0.930	0.939	0.984	0.943
	Δq (%)	0.58	1.18	0.38	0.36
PSO	q_e (mg/g)	125.0	108.7	110.6	117.6
	K_2 (1/min)	0.00015	0.0003	0.00036	0.00035
	R^2	0.997	0.999	0.973	0.987
	Δq (%)	1.72	0.33	0.09	0.18
Elovich	α [mg/g·min]	2.11			
		3.44	3.18	4.26	
	β [g/mg]	0.045	0.066	0.061	0.067
	R^2	0.875	0.847	0.875	0.771
	Δq (%)	6.68	10.5	9.76	11.7
IPD	K_{IPD} [mg/g·min$^{0.5}$]	0.13	0.089	0.092	0.12
	C [mg/g]	52.3	62.2	61.7	52.3
	R^2	0.777	0.727	0.758	0.777

Fig. 7. Mechanism of mass transfer process using CC_1_DES.

mathematical models of continuous adsorption, including the Thomas, Yoon-Nelson, and Adams–Bohart models, to examine the adsorption performance. The Thomas model is widely recognized for its ability to depict the performance of columns and breakthrough curves. This model is based on Langmuir adsorption-desorption isotherms for equilibrium and second-order reversible reaction kinetics for the rate driving force, with no external or intraparticle diffusion limitations. The Thomas model is characterized by plug flow behavior within the bed [75]. The Yoon-Nelson model is based on the idea that the rate at which the probability of adsorption diminishes for each adsorbate molecule is proportional to the probability of adsorbate adsorption and probability of adsorbate breakthrough on the adsorbent. This model was developed to minimize the error associated with employing the Thomas model, particularly during lower or higher periods of the breakthrough curve. The Adams-Bohart model posits that the adsorption rate is directly proportional to both the residual capacity of the adsorbent and the concentration of the adsorbing species and is commonly utilized to describe the initial portion of the breakthrough curve.

The predicted parameters of all models for the VSC indicated that the best fit was obtained for the two compatible models of Yoon-Nelson and Thomas. In contrast, the smallest fit based on R^2 values was obtained for the Adams-Bohart model. The predicted parameters for all the VSCs are provided in Table 2. In contrast, a comparison of the sorption capacities shows that the most reliable results are obtained by fitting the Adams-Bohart model for most VSCs. All models overestimated the adsorption capacities of CC_1_DES compared with the experimental values. However, the Δq did not exceed 12.4%. According to the Yoon-Nelson model, the predicted half-breakthrough times (τ) were close to the experimental data: 299.1, 328.3, 337.4 and 372.0 min for CS_2, IPM, PM and DMDS, respectively. The predicted parameter values are beneficial for designing practical engineering applications. Furthermore, the adsorption rate constant (K_{YN}) decreased with increasing molecular diameter of VSCs. This can be explained by the fact that the superimposed pore wall force was enhanced with an increase in the adsorbate molecule diameter. Owing to this interference force, the diffusion effect of the adsorption process significantly increases, which may result in a decrease in the adsorption rates of the VSCs [70,76]. The Thomas model resulted in a slightly lower sorption capacity. This is because the Thomas model is specifically designed for adsorption systems, where internal and external diffusion are not limiting steps. The presence of a DES layer on the surface of the biosorbent renders this model less favorable for predicting the adsorption process. The fit to the Adams-Bohart (I) model for the entire adsorption curve was very low, with R^2 values ranging from 0.82 0.89. This is because The Adams-Bohart model is useful for the simulation of fixed-bed adsorption columns and suitable for characterizing the initial part of the breakthrough curve [77,78]. Therefore, in further considerations, curves up to 240 min of running the process (Adams-Bohart (II)) were used, for which R2 values were 0.95-0.99. The results indicated that the adsorption rate constants (K_{AB}) were 0.033, 0.04, 0.042, and 0.046 L/(min·mg) respectively for CS_2, IPM, PM and DMDS. Meanwhile, the maximum VSCs adsorption capacity per unit volume of the adsorbent column was 96.7, 95.0, 93.8, 97.3 mg/L, respectively. These values are of the same order as the adsorption capacities under real conditions, as well as the overhanging solubility

Table 2
Results of fixed-bed column prediction for adsorption of selected VSCs.

Kinetic model	Parameter	CS_2	IPM	PM	DMDS
Thomas model	K_{Th} (mL/(min·mg))	0.51	0.42	0.42	0.41
	q_{mod} [mg/g]	116.8	134.8	135.5	134.0
	R^2	0.966	0.965	0.957	0.957
	Δq (%)	2.6	9.9	9.3	6.5
Yoon-Nelson model	K_{YN} (1/min)	0.006	0.0049	0.005	0.0049
	t [min]	316.7	365.5	367.3	363.3
	q_{mod} [mg/g]	113.8	131.3	129.7	134.0
	R^2	0.966	0.965	0.957	0.957
	Δq (%)	1.7	8.8	7.5	6.5
Adams-Bohart model (I)	K_{AB} (L/(min·mg))	0.021	0.023	0.020	0.022
	N_0 [mg/L]	148.7	124.2	131.5	133.1
	R^2	0.895	0.857	0.828	0.827
Adams-Bohart model (II)	K_{AB} (L/(min·mg))	0.037	0.04	0.042	0.046
	N_0 [mg/L]	96.7	95.0	93.8	97.3
	R^2	0.996	0.954	0.949	0.958

values of VSCs in DES. This is because in the first stage, there is an external diffusion process of VSCs in the DES layer.

3.5. Regeneration processes

In industrial applications, one of the most critical factors for adsorbents is their ability to be repeatedly regenerated with a minimal loss of adsorption capacity. Because the adsorption process is exothermic, heating the adsorbent shifts the equilibrium of the process toward desorption. The higher the temperature, the more efficient the desorption process. However, the temperature must not be too high to prevent the degradation or evaporation of DES from the surface of the biosorbent. Hence, a temperature of 110 °C was selected based on the TGA results. This temperature is higher than the boiling point of all tested VSCs and lower than the decomposition temperature of CC_1_DES. To evaluate this capability, a series of five adsorption-desorption cycles were performed. After each cycle, the adsorption capacity of the VSCs was assessed and FT-IR spectra were acquired to confirm any potential changes in the structural features of the biosorbent (Figure S7). The results demonstrated that even after five cycles, the process efficiency remained high, with only a slight decrease of approximately 6.2%. In the FT-IR spectra, the characteristic peaks of the VSCs were evident after adsorption. The peaks at 2586 and 952 cm^{-1} correspond to S-H stretching from PM and IPM, and C-S stretching from DMDS, respectively. Additionally, a band originating from the C=S thiocarbonyl functionality of CS_2 at 1096-1118 cm^{-1} was also observed. However, the intensity of this band is not visible because of the less polar nature of the C=S bonds. Furthermore, a shift of the hydroxyl group band towards higher values from 3336 to 3350 cm^{-1} was observed, indicating the formation of hydrogen bonds between the biosorbent and the adsorbed pollutants. This is likely due to the attachment of carbon dioxide, which can form strong non-covalent bonds with hydroxyl groups on the surface of the biosorbent. The biosorbent samples showed no sulfur compound peaks after the regeneration processes, suggesting that the process was complete, and the surface structure remained unchanged. In addition, the adsorption capacity remained almost unchanged even after five

adsorption-desorption cycles.

3.6. Comparison with literature data

Owing to the limited number of studies focused on the adsorption of volatile organosulfur compounds using biosorbents, a direct comparison of the individual compounds examined in this research is challenging. To date, only one study has investigated the use of biochar prepared from biosorbents (coconut shell, oak, poultry litter, and swine manure) for the adsorption of DMDS. The biosorbents were subjected to pyrolysis at temperatures ranging from 350 °C to 700°C. However, the adsorption capacity for DMDS reached a peak of 13.4 mg/g, which was considerably lower than the values demonstrated by the biosorbents evaluated in this study. Higher sorption capacities were obtained for PM using coconut shells modified with CuO, which was 33.3 - 71.4 mg/g. Similar results were obtained for other VSCs that were not studied in the present work, such as methyl mercaptan (MM) and dimethyl trisulfide (DMTS). Because of the small number of studies that have focused on using biosorbents to eliminate VSCs, the results for other types of adsorbents, such as zeolites (5A, 13X), iron oxide (IO), iron hydroxide (IH), silica gel (SG), activated carbon (AC), and Nyex A, are compiled and presented in Table 3. Similar sorption capacities to DES-modified biosorbents were obtained for activated carbons subjected to nitric oxidation and oxygen activation; however, the matrix effect was not investigated in this work, as the VSCs were removed from a pure inert gas, nitrogen. In addition, many studies have not considered the possibility of regeneration, which is one of the most important parameters affecting the practical applications of adsorbents.

3.7. Techno-economic analysis

Techno-economic costs were estimated based on previous studies [85,86]. The production and capital costs were estimated for 1 kg of new biosorbents. The estimates include both the preparation of the adsorbent and the costs associated with its modification. The estimated values are listed in Table 4. The production and capital costs were estimated for

Table 3
Comparison of new biosorbent modified with DES with literature data.

Sorbent/biosorbent	Sorbent preparation	VSCs	Gas matrix	Sorption capacity (mg/g)	Regeneration cycles	Ref.
Oak	Pyrolysis (N_2, 500 °C)	DMDS, DMTS	N_2	0.45 (DMDS) 0.11 (DMTS)	n.d.	[79]
Corn starch	Carbonization (400 °C, 3 h, N_2) and KOH activation (800 °C, 12 h)	MM	N_2	78.16 (MM)	5	[80]
Coconut shell modified with CuO at 0.25 M	Steam physical activation (800 °C), pre-treatment (HNO_3 3-6 M), modification (HNO_3 and Cu $(NO_3)_2$)	PM	N_2	33.3 – 71.4 (PM)	n.d.	[81]
IO IH AC Zeolite (5A), and zeolite (13x) Silica gel (A2)	Commercially available adsorbents	CS_2	$CH_4:CO_2$ (69:30 % v/v) and H_2S (1900 ppm), COS (100 ppm), CS_2 (100 ppm), D4 (10 ppm), D5 (20 ppm)	0.41 (CS_2) 0.43 (CS_2) 26.42 (CS_2) 22.5 and 15.27 (CS_2) 0.78 (CS_2)	n.d.	[82]
AC	Nitric oxidation (HNO_3, 6 N) and oxygen activation (O_3)	ETM DMS MDS	N_2	16 – 103 (ETM) 8 – 21 (DMS) 108 – 142 (DMDS)	n.d.	[12]
Nyex 1000	Commercially available adsorbent	IPM	N_2	0.17	1	[83]
Silver exchanged Y zeolites (AgNa-Y)	AgNa-Y was prepared from Na-Y using ion-exchange procedure with an aqueous solution of silver nitrate and calcining (400 °C)	DMS TBM	Natural gas	1.9 mmol/g (DMS) 1.9 mmol/g (TBM)	1	[84]
Corn cobs modified by DES	Water purification and DES impregnation	CS_2, PM, IPM, DMDS	$CH_4:CO_2:N_2$ (60.2:30:9.8 % v/v)	108.3 (CS_2) 103.8 (IPM) 105.9 (PM) 112.1 (DMDS)	5	This study

AC - activated carbons; DMS – dimethlysulfide; DMTS – dimethyl trisulfide; ETM - Ethyl mercaptan; IH - iron hydroxides; IO - iron oxide; MM - Methyl mercaptan; n.d. - no data; TBM - t-butylmercaptan.

Table 4
Estimated cost of producing 1 kg of DES-modified biosorbent.

Parameter	Estimated cost ($/kg)
Cost of adsorbent production	
Equipment	0.5
Technical and installation cost	0.1
Power source	0.002
Chemicals for surface modification	3.13
Feed stock (corn cobs waste)	0.1
Drying, sieving, and transportation	0.007
Sum of adsorbent production	**3.739**
Capital cost	
Maintenance cost	0.01
Laborer cost	0
Fixed assets cost	0.01
Extra cost	0.015
Sum of capital cost	**0.035**
Total cost	**3.77**

different cases, including equipment, utility, maintenance, fixed and extra costs. Owing to the use of waste, it was assumed that there is no cost associated with the purchase of biosorbents (waste corn cobs). However, it was assigned a cost of $0.1, which included, among other things, the cost associated with waste collection [87]. Reagents for the synthesis of DES per 100 mL after taking into account TPABr and HD in a molar ratio of 1:3 was $27.4. The calculation includes the cost of high-purity desensitizers sold in retail. The wholesale purchase was an average of 10 % of the price. In addition, the purchase of ethanol, which is needed for the preparation of DES at a cost as of 14/03/2024 is $0.43 per gallon, was included. The estimated installation and technical costs were calculated to be 20 % of the total cost of the equipment. The cost of drying and sieving, on the other hand, was assumed based on calculations from another study. In addition to total capital cost, the total capital cost was estimated to be $0.085, which comprised maintenance, labor, and fixed asset expenses. These costs were estimated to be $0.035. The total cost of producing 1 kg of new biosorbents is $3.87. The cost of the modified biosorbent is higher than that of other adsorbents such as activated carbon ($0.45). However, the price of activated carbon production considers industrial production per 1 kg, hence the price is much lower. This correlates with the fact that, as the production volume increases, the price of the final product decreases [87]. The biggest impact on the cost of producing a new sorbent is the synthesis of DES, which are currently not commercially available. In addition, the calculation does not consider the possibility of reuse of the sorbent after regeneration, which also significantly affects the cost of the entire process.

4. Conclusion

The aim of the present study was to apply DES-modified lignocellulosic waste as a new class of adsorbents for efficient biogas desulfurization. The results showed that corncob-based adsorbents modified with tetrapropylammonium bromide: 1,2-hexanediol (1:3) exhibited the highest sorption capacities. The sorption capacities of the individual VSCs were 108.3, 103.8, 105.9, and 112.1 mg/g for CS_2, IPM, PM, and DMDS, respectively. These values are significantly higher than those reported in the literature. Moreover, the negligible sorption capacities of methane and carbon dioxide, combined with the low cost of obtaining sorbents, suggest the great potential of new biosorbents for upgrading biogas. In addition, the application of waste materials as a new sorbent fits the trends of sustainable development and green engineering. The adsorption process using the new biosorbent can be described by the PSO kinetic model, as well as the Yoon-Nelson and Adams-Bohart models. Most likely, the proposed biogas desulfurization process occurs as a result of a combination of adsorption in solid corncob waste and absorption in a thin layer of deep eutectic solvent.

CRediT authorship contribution statement

Patrycja Makoś-Chełstowska: Conceptualization, Formal analysis, Funding acquisition, Methodology, Project administration, Resources, Supervision, Validation, Visualization, Writing – original draft, Writing – review & editing. **Dominika Sikorska:** Data curation, Investigation, Writing – original draft. **Patrycja Janicka:** Data curation, Investigation, Writing – original draft. **Edyta Słupek:** Data curation, Investigation, Writing – original draft. **Aleksandra Mielewczyk-Gryń:** Investigation, Writing – original draft. **Jacek Gębicki:** Supervision, Writing – review & editing.

Declaration of competing interest

The authors declare that they have no known competing financial interests or personal relationships that could have appeared to influence the work reported in this paper.

Data availability

Data will be made available on request.

Appendix A. Supplementary data

Supplementary data to this article can be found online at https://doi.org/10.1016/j.cej.2024.152639.

References

[1] Y. Li, C.P. Alaimo, M. Kim, N.Y. Kado, J. Peppers, J. Xue, C. Wan, P.G. Green, R. Zhang, B.M. Jenkins, C.F.A. Vogel, S. Wuertz, T.M. Young, M.J. Kleeman, Composition and toxicity of biogas produced from different feedstocks in California, Environ. Sci. Technol. (2019), https://doi.org/10.1021/acs.est.9b03003.

[2] F.A.T. Andersson, A. Karlsson, B.H. Svensson, J. Ejlertsson, Occurrence and abatement of volatile sulfur compounds during biogas production, J. Air Waste Manag. Assoc. 54 (2004) 855–861, https://doi.org/10.1080/10473289.2004.10470953.

[3] E. Smet, P. Lens, H. Van Langenhove, Treatment of waste gases contaminated with odorous sulfur compounds, Crit. Rev. Environ. Sci. Technol. 28 (1998) 89–117, https://doi.org/10.1080/10643389891254179.

[4] A. De Angelis, Natural gas removal of hydrogen sulphide and mercaptans, Appl. Catal. B Environ. 113–114 (2012) 37–42, https://doi.org/10.1016/J.APCATB.2011.11.026.

[5] C.L. Lee, P. Brimblecombe, Anthropogenic contributions to global carbonyl sulfide, carbon disulfide and organosulfides fluxes, Earth-Science Rev. 160 (2016) 1–18, https://doi.org/10.1016/J.EARSCIREV.2016.06.005.

[6] O.W. Awe, Y. Zhao, A. Nzihou, D.P. Minh, N. Lyczko, A review of biogas utilisation, purification and upgrading technologies, Waste and Biomass Valorization. 8 (2017) 267–283, https://doi.org/10.1007/s12649-016-9826-4.

[7] S. Rasi, J. Läntelä, A. Veijanen, J. Rintala, Landfill gas upgrading with countercurrent water wash, Waste Manag. 28 (2008) 1528–1534, https://doi.org/10.1016/j.wasman.2007.03.032.

[8] A. Janssen, P.L.F. Van Den Bosch, R.C. Van Leerdam, M. De Graaff, Bioprocesses for the removal of volatile sulfur compounds from gas streams, Air Pollut. Prev. Control Bioreact. Bioenergy. (2013) 247–274, https://doi.org/10.1002/9781118523360.ch11.

[9] K. Barbusinski, K. Kalemba, D. Kasperczyk, K. Urbaniec, V. Kozik, Biological methods for odor treatment – A review, J. Clean. Prod. 152 (2017) 223–241, https://doi.org/10.1016/J.JCLEPRO.2017.03.093.

[10] E. Hunter-Sellars, J.J. Tee, I.P. Parkin, D.R. Williams, Adsorption of volatile organic compounds by industrial porous materials: Impact of relative humidity, Microporous Mesoporous Mater. 298 (2020) 110090, https://doi.org/10.1016/j.micromeso.2020.110090.

[11] A.B. Fuertes, G. Marbán, D.M. Nevskaia, Adsorption of volatile organic compounds by means of activated carbon fibre-based monoliths, Carbon N. Y. 41 (2003) 87–96, https://doi.org/10.1016/S0008-6223(02)00274-9.

[12] E. Vega, J. Lemus, A. Anfruns, R. Gonzalez-Olmos, J. Palomar, M.J. Martin, Adsorption of volatile sulphur compounds onto modified activated carbons: Effect of oxygen functional groups, J. Hazard. Mater. 258–259 (2013) 77–83, https://doi.org/10.1016/j.jhazmat.2013.04.043.

[13] H. Kim, K.J. Ko, M. Mofarahi, K.M. Kim, C.H. Lee, Adsorption behavior and mechanism of ultra-low concentration sulfur compounds in natural gas on Cu-impregnated activated carbon, Chem. Eng. J. 470 (2023) 144274, https://doi.org/10.1016/j.cej.2023.144274.

[14] W.K. Pui, R. Yusoff, M.K. Aroua, A review on activated carbon adsorption for volatile organic compounds (VOCs), Rev. Chem. Eng. 35 (2019) 649–668, https://doi.org/10.1515/revce-2017-0057.

[15] X. Li, L. Zhang, Z. Yang, P. Wang, Y. Yan, J. Ran, Adsorption materials for volatile organic compounds (VOCs) and the key factors for VOCs adsorption process: A review, Sep. Purif. Technol. 235 (2020) 116213, https://doi.org/10.1016/J.SEPPUR.2019.116213.

[16] J. Wu, X. Zhu, F. Yang, R. Wang, T. Ge, Shaping techniques of adsorbents and their applications in gas separation: a review, J. Mater. Chem. A. 10 (2022) 22853–22895, https://doi.org/10.1039/d2ta04352a.

[17] S. Lu, Q. Liu, R. Han, M. Guo, J. Shi, C. Song, N. Ji, X. Lu, D. Ma, Potential applications of porous organic polymers as adsorbent for the adsorption of volatile organic compounds, J. Environ. Sci. 105 (2021) 184–203, https://doi.org/10.1016/J.JES.2021.01.007.

[18] V. Kumar, Y.S. Lee, J.W. Shin, K.H. Kim, D. Kukkar, Y. Fai Tsang, Potential applications of graphene-based nanomaterials as adsorbent for removal of volatile organic compounds, Environ. Int. 135 (2020) 105356, https://doi.org/10.1016/j.envint.2019.105356.

[19] M.I. Severino, A. Al Mohtar, C. Vieira Soares, C. Freitas, N. Sadovnik, S. Nandi, G. Mouchaham, V. Pimenta, F. Nouar, M. Daturi, G. Maurin, M.L. Pinto, C. Serre, MOFs with Open Metal(III) Sites for the Environmental Capture of Polar Volatile Organic Compounds, Angew. Chemie - Int. Ed. 62 (2023), https://doi.org/10.1002/anie.202211583.

[20] B. Siu, A.R. Chowdhury, Z. Yan, S.M. Humphrey, T. Hutter, Selective adsorption of volatile organic compounds in metal-organic frameworks (MOFs), Coord. Chem. Rev. 485 (2023) 215119, https://doi.org/10.1016/j.ccr.2023.215119.

[21] G. Kumari, A. Guleria, K. Singh, N. Kumar, A. Guleria, D. Kumar, E. Lima, Lignocellulosic biopolymers as potential biosorbents, Biomass, Biofuels, Biochem. Biochem. Mater. Prod. from Sustain. Biomass Resour. (2022) 391–429, https://doi.org/10.1016/B978-0-12-824419-7.00022-4.

[22] K. Asemave, L. Thaddeus, P.T. Tarhemba, Lignocellulosic-based sorbents: a review, Sustain. Chem. 2 (2021) 271–285, https://doi.org/10.3390/suschem2020016.

[23] S. Ghanbari, C.H. Niu, Equilibria of lignocellulose biosorbents for gas dehydration, Sep. Purif. Technol. 227 (2019) 115668, https://doi.org/10.1016/j.seppur.2019.06.006.

[24] Z.T. Chong, L.S. Soh, W.F. Yong, Valorization of agriculture wastes as biosorbents for adsorption of emerging pollutants: Modification, remediation and industry application, Results Eng. 17 (2023) 100960, https://doi.org/10.1016/J.RINENG.2023.100960.

[25] A.P. Abbott, G. Capper, D.L. Davies, R.K. Rasheed, V. Tambyrajah, Novel solvent properties of choline chloride/urea mixtures, Chem. Commun. (2003) 70–71, https://doi.org/10.1039/b210714g.

[26] E.L. Smith, A.P. Abbott, K.S. Ryder, Deep eutectic solvents (DESs) and their applications, Chem. Rev. 114 (2014) 11060–11082, https://doi.org/10.1021/cr300162p.

[27] Z. Ghazali, N. Suhaili, M.N.A. Tahari, M.A. Yarmo, N.H. Hassan, R. Othaman, Impregnating deep eutectic solvent choline chloride:urea:polyethyleneimine onto mesoporous silica gel for carbon dioxide capture, J. Mater. Res. Technol. 9 (2020) 3249–3260, https://doi.org/10.1016/J.JMRT.2020.01.073.

[28] T. Ariyanto, K. Masruroh, G.Y.S. Pambayun, N.I.F. Mukti, R.B. Cahyono, A. Prasetya, I. Prasetyo, Improving the Separation of CO2/CH4 Using Impregnation of Deep Eutectic Solvents on Porous Carbon, ACS Omega. 6 (2021) 19194–19201, https://doi.org/10.1021/acsomega.1c02545.

[29] N. Noorani, A. Mehrdad, Impregnation of amine functionalized deep eutectic solvents in NH2-MIL-53(Al) MOF for CO2/N2 separation, Sci. Rep. 13 (2023) 1–17, https://doi.org/10.1038/s41598-023-40191-9.

[30] P. Makoś, E. Słupek, A. Małachowska, Silica Gel Impregnated by Deep Eutectic Solvents for Adsorptive Removal of BTEX from Gas Streams, Materials (Basel). 13 (2020) 1894, https://doi.org/10.3390/ma13081894.

[31] P. Makoś-Chełstowska, K. Kucharska, E. Słupek, J. Gębicki, M. de la Guardia, Magnetic deep eutectic solvents as efficient media for extraction of furfural and 5-hydroxymethylfurfural from aqueous samples, J. Mol. Liq. 390 (2023), https://doi.org/10.1016/j.molliq.2023.122945.

[32] P. Makoś-Chełstowska, E. Słupek, J. Gębicki, Deep eutectic solvent-based green absorbents for the effective removal of volatile organochlorine compounds from biogas, Green Chem. (2021) 4814–4827, https://doi.org/10.1039/d1gc01735g.

[33] K. Kucharska, H. Cieśliński, P. Rybarczyk, E. Słupek, R. Łukajtis, K. Wychodnik, M. Kamiński, Fermentative conversion of two-step pre-treated lignocellulosic biomass to hydrogen, Catalysts. 9 (2019), https://doi.org/10.3390/catal9100858.

[34] A. Sluiter, B. Hames, R. Ruiz, C. Scarlata, J. Sluiter, D. Templeton, D. Crocker, Determination of structural carbohydrates and lignin in Biomass - NREL/TP-510-42618, Natl. Renew. Energy Lab. (2008) 17.

[35] P. Makoś-Chełstowska, E. Słupek, A. Małachowska, Superhydrophobic sponges based on green deep eutectic solvents for spill oil removal from water, J. Hazard. Mater. 425 (2022) 127972, https://doi.org/10.1016/j.jhazmat.2021.127972.

[36] P. Makoś-Chełstowska, E. Słupek, Superhydrophobic and superoleophilic melamine sponges impregnated with deep eutectic solvents for oil spill cleanup, Sep. Purif. Technol. 324 (2023) 124537, https://doi.org/10.1016/j.seppur.2023.124537.

[37] N. Bhardwaj, A.N. Bhaskarwar, A review on sorbent devices for oil-spill control, Environ. Pollut. 243 (2018) 1758–1771, https://doi.org/10.1016/J.ENVPOL.2018.09.141.

[38] P. Makoś-Chełstowska, E. Słupek, A. Mielewczyk-Gryń, T. Klimczuk, Magnetic superhydrophobic melamine sponges for crude oil removal from water, Chemosphere. 346 (2024), https://doi.org/10.1016/j.chemosphere.2023.140533.

[39] T. Hong, L. Wei, K. Cui, Y. Dong, R.L. Li, T. Zhang, Y. Zhao, L. Luo, Adsorption performance of volatile organic compounds on activated carbon fibers in a fixed bed column, J. Environ. Chem. Eng. 9 (2021) 106347, https://doi.org/10.1016/J.JECE.2021.106347.

[40] K.N. Gupta, R. Kumar, Kinetic modeling and optimization of fraction of bed utilized for the gaseous phase removal of toluene in fixed bed adsorption column: Response surface methodology, Sep. Sci. Technol. 55 (2020) 1062–1077, https://doi.org/10.1080/01496395.2019.1583252.

[41] F.C. Wu, R.L. Tseng, R.S. Juang, Characteristics of Elovich equation used for the analysis of adsorption kinetics in dye-chitosan systems, Chem. Eng. J. 150 (2009) 366–373, https://doi.org/10.1016/j.cej.2009.01.014.

[42] L. Largitte, R. Pasquier, A review of the kinetics adsorption models and their application to the adsorption of lead by an activated carbon, Chem. Eng. Res. Des. 109 (2016) 495–504, https://doi.org/10.1016/j.cherd.2016.02.006.

[43] J.I. Salazar Gómez, H. Lohmann, J. Krassowski, Determination of volatile organic compounds from biowaste and co-fermentation biogas plants by single-sorbent adsorption, Chemosphere. 153 (2016) 48–57, https://doi.org/10.1016/J.CHEMOSPHERE.2016.02.128.

[44] E. Słupek, P. Makoś, Absorptive desulfurization of model biogas stream using choline chloride-based deep eutectic solvents, Sustainability. 12 (2020) 1619–1635, https://doi.org/10.3390/su12041619.

[45] Z. Yang, K.R. Gluesenkamp, A. Frazzica, Equilibrium vapor pressure properties for absorbent and adsorbent materials, Int. J. Refrig. 124 (2021) 134–166, https://doi.org/10.1016/J.IJREFRIG.2020.12.013.

[46] K. Xin, I. Roghair, F. Gallucci, M. van Sint Annaland, Total vapor pressure of hydrophobic deep eutectic solvents: experiments and modelling, J. Mol. Liq. 325 (2021) 115227, https://doi.org/10.1016/J.MOLLIQ.2020.115227.

[47] B. Ozturk, J. Gonzalez-Miquel, Alkanediol-based deep eutectic solvents for isolation of terpenoids from citrus essential oil: experimental evaluation and COSMO-RS studies, Sep. Purif. Technol. 227 (2019) 115707, https://doi.org/10.1016/J.SEPPUR.2019.115707.

[48] E. Słupek, P. Makoś-Chełstowska, J. Gębicki, Removal of siloxanes from model biogas by means of deep eutectic solvents in absorption process, Materials (Basel). 14 (2021) 1–20, https://doi.org/10.3390/ma14020241.

[49] R.M. Ojeda, F. Llovell, Soft-SAFT transferable molecular models for the description of gas solubility in eutectic ammonium salt-based solvents, J. Chem. Eng. Data. 63 (2018) 2599–2612, https://doi.org/10.1021/acs.jced.7b01103.

[50] Y. Chu, X. He, MoDoop: an automated computational approach for COSMO-RS prediction of biopolymer solubilities in ionic liquids, ACS Omega. 4 (2019) 2337–2343, https://doi.org/10.1021/acsomega.8b03255.

[51] F. Chemat, H. Anjum, A.M. Shariff, P. Kumar, T. Murugesan, Thermal and physical properties of (Choline chloride + urea + l-arginine) deep eutectic solvents, J. Mol. Liq. 218 (2016) 301–308, https://doi.org/10.1016/J.MOLLIQ.2016.02.062.

[52] A. Hayyan, F.S. Mjalli, I.M. Alnashef, T. Al-Wahaibi, Y.M. Al-Wahaibi, M.A. Hashim, Fruit sugar-based deep eutectic solvents and their physical properties, Thermochim. Acta. 541 (2012) 70–75, https://doi.org/10.1016/j.tca.2012.04.030.

[53] Q. Zhang, K. De Oliveira Vigier, S. Royer, F. Jérôme, Deep eutectic solvents: Syntheses, properties and applications, Chem. Soc. Rev. 41 (2012) 7108–7146, https://doi.org/10.1039/c2cs35178a.

[54] J. Cao, E. Su, Hydrophobic deep eutectic solvents: the new generation of green solvents for diversified and colorful applications in green chemistry, J. Clean. Prod. 314 (2021) 127965, https://doi.org/10.1016/J.JCLEPRO.2021.127965.

[55] P. Makoś, E. Słupek, J. Gębicki, Hydrophobic deep eutectic solvents in microextraction techniques–A review, Microchem. J. 152 (2020) 104384, https://doi.org/10.1016/j.microc.2019.104384.

[56] P. Makoś-Chełstowska, M. Kaykhaii, J. Płotka-Wasylka, M. de la Guardia, Magnetic deep eutectic solvents – Fundamentals and applications, J. Mol. Liq. 365 (2022) 120158, https://doi.org/10.1016/J.MOLLIQ.2022.120158.

[57] R. Haghbakhsh, K. Parvaneh, S. Raeissi, A. Shariati, A general viscosity model for deep eutectic solvents: The free volume theory coupled with association equations of state, Fluid Phase Equilib. 470 (2018) 193–202, https://doi.org/10.1016/j.fluid.2017.08.024.

[58] M.C. Timar, A. Varodi, M. Hacibektasoglu, M. Campean, Color and FTIR analysis of chemical changes in beech wood (Fagus sylvatica L.) after light steaming and heat treatment in two different environments, BioResources. 11 (2016) 8325–8343, https://doi.org/10.15376/biores.11.4.8325-8343.

[59] R. Ding, H. Wu, M. Thunga, N. Bowler, M.R. Kessler, Processing and characterization of low-cost electrospun carbon fibers from organosolv lignin/polyacrylonitrile blends, Carbon N. Y. 100 (2016) 126–136, https://doi.org/10.1016/J.CARBON.2015.12.078.

[60] R. Chromá, M. Vilková, I. Shepa, P. Makoś-Chełstowska, V. Andruch, Investigation of tetrabutylammonium bromide-glycerol-based deep eutectic solvents and their mixtures with water by spectroscopic techniques, J. Mol. Liq. 330 (2021) 115617, https://doi.org/10.1016/j.molliq.2021.115617.

[61] A. Shishov, P. Makoś-Chełstowska, A. Bulatov, V. Andruch, Deep Eutectic Solvents or Eutectic Mixtures? Characterization of Tetrabutylammonium Bromide and Nonanoic Acid Mixtures, J. Phys. Chem. B. 126 (n.d.) 3889–3896. https://doi.org/10.1021/acs.jpcb.2c00858.

[62] H. Yang, R. Yan, H. Chen, D.H. Lee, C. Zheng, Characteristics of hemicellulose, cellulose and lignin pyrolysis, Fuel. 86 (2007) 1781–1788, https://doi.org/10.1016/J.FUEL.2006.12.013.

[63] R.K. Mishra, K. Mohanty, Characterization of non-edible lignocellulosic biomass in terms of their candidacy towards alternative renewable fuels, Biomass Convers. Biorefinery. 8 (2018) 799–812, https://doi.org/10.1007/s13399-018-0332-8.

[64] E. Galiwango, N.S. Abdel Rahman, A.H. Al-Marzouqi, M.M. Abu-Omar, A.A. Khaleel, Isolation and characterization of cellulose and α-cellulose from date palm biomass waste, Heliyon. 5 (2019) e02937.

[65] P. Makoś, G. Boczkaj, Deep eutectic solvents based highly efficient extractive desulfurization of fuels – Eco-friendly approach, J. Mol. Liq. 296 (2019) 111916–111927, https://doi.org/10.1016/j.molliq.2019.111916.

[66] E.D. Revellame, D.L. Fortela, W. Sharp, R. Hernandez, M.E. Zappi, Adsorption kinetic modeling using pseudo-first order and pseudo-second order rate laws: A review, Clean. Eng. Technol. 1 (2020) 100032, https://doi.org/10.1016/J.CLET.2020.100032.

[67] S. Guo, Z. Wang, S. Wu, Y. Cai, J. Zhang, C. Lou, W. Zhao, Modification of the adsorption model for the mixture of odor compounds and VOCs on activated Carbon: Insights from pore size distribution, Sep. Purif. Technol. 339 (2024) 126669, https://doi.org/10.1016/j.seppur.2024.126669.

[68] K.J. Hwang, W.G. Shim, Y. Kim, G. Kim, C. Choi, S.O. Kang, D.W. Cho, Dye adsorption mechanisms in TiO2 films, and their effects on the photodynamic and photovoltaic properties in dye-sensitized solar cells, Phys. Chem. Chem. Phys. 17 (2015) 21974–21981, https://doi.org/10.1039/c5cp03416g.

[69] K.L. Tan, B.H. Hameed, Insight into the adsorption kinetics models for the removal of contaminants from aqueous solutions, J. Taiwan Inst. Chem. Eng. 74 (2017) 25–48, https://doi.org/10.1016/j.jtice.2017.01.024.

[70] D. Zhang, J. Cao, G. Wu, L. Cui, Dynamic adsorption model fitting studies of typical VOCs using commercial activated carbon in a fixed bed, Water. Air. Soil Pollut. 229 (2018), https://doi.org/10.1007/s11270-018-3763-8.

[71] K.H. Chu, Breakthrough curve analysis by simplistic models of fixed bed adsorption: In defense of the century-old Bohart-Adams model, Chem. Eng. J. 380 (2020) 122513, https://doi.org/10.1016/J.CEJ.2019.122513.

[72] Q. Hu, Y. Xie, Z. Zhang, Modification of breakthrough models in a continuous-flow fixed-bed column: Mathematical characteristics of breakthrough curves and rate profiles, Sep. Purif. Technol. 238 (2020) 116399, https://doi.org/10.1016/J.SEPPUR.2019.116399.

[73] F.J. Gutiérrez Ortiz, M. Barragán Rodríguez, R.T. Yang, Modeling of fixed-bed columns for gas physical adsorption, Chem. Eng. J. 378 (2019) 121985, https://doi.org/10.1016/J.CEJ.2019.121985.

[74] M.S. Shafeeyan, W.M.A. Wan Daud, A. Shamiri, A review of mathematical modeling of fixed-bed columns for carbon dioxide adsorption, Chem. Eng. Res. Des. 92 (2014) 961–988, https://doi.org/10.1016/J.CHERD.2013.08.018.

[75] H.C. Thomas, Heterogeneous Ion Exchange in a Flowing System, J. Am. Chem. Soc. 66 (1944) 1664–1666, https://doi.org/10.1021/ja01238a017.

[76] P. Liu, H. Zhang, H. Xiang, Y. Yan, Adsorption separation for high purity propane from liquefied petroleum gas in a fixed bed by removal of alkanes, Sep. Purif. Technol. 158 (2016) 1–8, https://doi.org/10.1016/J.SEPPUR.2015.12.003.

[77] V. Sarin, T.S. Singh, K.K. Pant, Thermodynamic and breakthrough column studies for the selective sorption of chromium from industrial effluent on activated eucalyptus bark, Bioresour. Technol. 97 (2006) 1986–1993, https://doi.org/10.1016/J.BIORTECH.2005.10.001.

[78] T.S. Singh, K.K. Pant, Equilibrium, kinetics and thermodynamic studies for adsorption of As(III) on activated alumina, Sep. Purif. Technol. 36 (2004) 139–147, https://doi.org/10.1016/S1383-5866(03)00209-0.

[79] O. Hwang, S.R. Lee, S. Cho, K.S. Ro, M. Spiehs, B. Woodbury, P.J. Silva, D.W. Han, H. Choi, K.Y. Kim, M.W. Jung, Efficacy of Different Biochars in Removing Odorous Volatile Organic Compounds (VOCs) Emitted from Swine Manure, ACS Sustain. Chem. Eng. 6 (2018) 14239–14247, https://doi.org/10.1021/acssuschemeng.8b02881.

[80] X. Yao, J. Zhou, Z. Liu, Study on adsorption of low-concentration methyl mercaptan by starch-based activated carbon, Chemosphere. 302 (2022) 134901, https://doi.org/10.1016/j.chemosphere.2022.134901.

[81] J.C. Moreno-Piraján, J. Tirano, B. Salamanca, L. Giraldo, Activated carbon modified with copper for adsorption of propanethiol, Int. J. Mol. Sci. 11 (2010) 927–942, https://doi.org/10.3390/ijms11030927.

[82] C.U. Bak, C.J. Lim, Y.D. Kim, W.S. Kim, Multi-stage adsorptive purification process for improving desulfurization performance of biogas, Sep. Purif. Technol. 227 (2019) 115702, https://doi.org/10.1016/j.seppur.2019.115702.

[83] M.G. Conti-Ramsden, H.M.A. Asghar, S.N. Hussain, E.P.L. Roberts, N.W. Brown, Removal of mercaptans from a gas stream using continuous adsorption-regeneration, Water Sci. Technol. 66 (2012) 1849–1855, https://doi.org/10.2166/wst.2012.383.

[84] S. Satokawa, Y. Kobayashi, H. Fujiki, Adsorptive removal of dimethylsulfide and t-butylmercaptan from pipeline natural gas fuel on Ag zeolites under ambient conditions, Appl. Catal. B Environ. 56 (2005) 51–56, https://doi.org/10.1016/j.apcatb.2004.06.022.

[85] T. Haeldermans, L. Campion, T. Kuppens, K. Vanreppelen, A. Cuypers, S. Schreurs, A comparative techno-economic assessment of biochar production from different residue streams using conventional and microwave pyrolysis, Bioresour. Technol. 318 (2020) 124083, https://doi.org/10.1016/j.biortech.2020.124083.

[86] E. Słupek, P. Makoś, J. Gębicki, Theoretical and economic evaluation of low-cost deep eutectic solvents for effective biogas upgrading to bio-methane, Energies. 13 (2020) 3379, https://doi.org/10.3390/en13133379.

[87] A. Mukherjee, J.A. Okolie, C. Niu, A.K. Dalai, Techno – Economic analysis of activated carbon production from spent coffee grounds: Comparative evaluation of different production routes, Energy Convers. Manag. X. 14 (2022) 100218, https://doi.org/10.1016/j.ecmx.2022.100218.